Application of a semiclassical model for the second-quantized many-electron Hamiltonian to nonequilibrium quantum transport: The resonant level model

David W.H. Swenson[1], Tal Levy[2], Guy Cohen[2], Eran Rabani[2] and William H. Miller[1]
[1] *Department of Chemistry and Kenneth S. Pitzer Center for Theoretical Chemistry, University of California, Berkeley, California 94720-1460, and Chemical Sciences Division, Lawrence Berkeley National Laboratory, Berkeley, California 94720-1460*
[2] *School of Chemistry, The Sackler Faculty of Exact Sciences, Tel Aviv University, Tel Aviv 69978, Israel*

(Dated: January 15, 2013)

A semiclassical (SC) approach is developed for nonequilibrium quantum transport in molecular junctions. Following the early work of Miller and White [*J. Chem. Phys.* **84**, 5059 (1986)], the many-electron Hamiltonian in second quantization is mapped onto a classical model that preserves the fermionic character of electrons. The resulting classical electronic Hamiltonian allows for real-time molecular dynamics simulations of the many-body problem from an uncorrelated initial state to the steady state. Comparisons with exact results generated for the resonant level model reveal that a semiclassical treatment of transport provides a quantitative description of the dynamics at all relevant timescales for a wide range of bias and gate potentials, and for different temperatures. The approach opens a door to treating nontrivial quantum transport problems that remain far from the reach of fully quantum methodologies.

I. INTRODUCTION

Molecular electronics[1] has provided means to study the dynamics of open quantum systems, in which one considers a small, strongly interacting and highly correlated region (the molecule and its closest vicinity) coupled to several large, noninteracting baths (representing the fermionic leads and environment). While the equilibrium nature of quantum dynamics in condensed phases has been mostly resolved,[2] the intrinsic nonequilibrium nature of transport through molecular junctions, along with the necessity to treat fermionic degrees of freedom, poses a much greater theoretical challenge, and thus remains poorly understood.

Several different paths have been taken to improve the standard Landauer-Büttiker approach[3,4] and its generalization to the multichannel case,[5] in order to account for electron-electron and electron-phonon correlations in molecular junctions. The different approaches can be classified as perturbative treatments, among which the most notable examples use the nonequilibrium Green's function (NEGF) formalism,[6,7] and numerically exact techniques, perhaps the most prominent of which have been time-dependent numerical renormalization group techniques[8–10] and the promising diagrammatic approaches based on path integral formulations.[11–16]

These approaches have been applied to a variety of physically interesting problems including the description of Coulomb and Franck-Condon blockade,[17–19] the nonequilibrium Kondo problem,[20,21] and inelastic electron tunneling.[11,22] While successful to a large extent, these approaches suffer from several limitations, including difficulties that arise in the treatment of more complex environments or when inelastic scattering is governed by interactions of electrons with soft modes that are dominated by large anharmonicities.

Parallel to these developments, a completely different paradigm has been devised based on semiclassical approaches. These have provided a useful tool to simulate the dynamics of molecular subsystems coupled to a fluctuating environment with significant anharmonicities. The most appealing semiclassical treatments have relied on the mixed quantum-classical approach[23–26] and on the semiclassical initial value representation.[27–29] The latter have been applied to a variety of physically interesting condensed phase problems with remarkable success.[30–41] It is interesting to note that such approaches have not received any attention in the context of nonequilibrium quantum transport, despite being exact in the harmonic boson case.[27,42,43]

A major goal of the present work is to show how a semiclassical (SC) approach can treat the dynamics of a many-body quantum system driven away from equilibrium by the application of a bias voltage. We describe the transport problem in second quantization, partitioning the space into an interacting region describing the molecule and its closest vicinity and a noninteracting region representing the leads and the environment. The approach is based on an SC model for the general second-quantized many-electron Hamiltonian by Miller and White (MW),[44] which followed earlier work of McCurdy, Meyer, and Miller (MMM)[45–48] on constructing classical models for electronic degrees of freedom. The essence of MW's model is that each fermionic degree of freedom (i.e., each pair of one-particle annihilation/creation operators) is described by a classical degree of freedom (pair of action-angle variables), while in MMM's earlier work each electronic *state* is described by a classical degree of freedom. MW's model is thus a more "microscopic" description of the electronic degrees of freedom, and more importantly much more "efficient" (i.e.,

involving many fewer classical degrees of freedom) for many electron systems (where the number of electronic states can be much larger than the number of one-particle annihilation/creation operators).

To assess the accuracy of the proposed approach, we focus on the resonant level model and derive working expressions to simulate the left, right and total current using classical trajectories with quasi-classical initial conditions. Remarkably excellent agreement in comparison to exact results is achieved for a wide range of bias and gate voltages and for different temperatures. Our approach provides a natural framework to study more complex molecular transport problems with promising performance.

The paper is organized as follows. In Section II we summarize the semiclassical procedure for constructing a classical model of a second quantized Hamiltonian. Section III describes the resonant level model, which is used as a test case to assess the accuracy of the semiclassical approach. Exact quantum mechanical results for the resonant level model are provided in Section IV. Section V summarizes the main results and provides a detailed comparison between the semiclassical approach and the exact quantum mechanical treatment. The comparisons cover a wide range of gate and bias potentials from high to low temperatures. Section VI summarizes and concludes.

II. SEMICLASSICAL APPROACH

A. Mapping

The approach that has been used[44,46–48] to construct semiclassical models for electronic degrees of freedom is to invert (as meaningfully as possible) the Heisenberg correspondence relation,

$$\left\langle n'\middle|\hat{A}\middle|n\right\rangle = (2\pi)^{-F}\int_0^{2\pi} e^{-i(n'-n)q} A_{\rm cl}(\bar{n},q)\mathrm{d}q \qquad (1)$$

where $\bar{n}=\frac{1}{2}(n'+n)$, F is the number of degrees of freedom, and $A_{\rm cl}(\bar{n},q)$ is a function of the classical action-angle variables. The Heisenberg correpondence relation was originally used to obtain approximate matrix elements for $\hat{A}$ from the corresponding classical function of action-angle variables; the semiclassical goal here is to obtain a classical function of action-angle variables that corresponds (as best as possible) to the given quantum mechanical matrix elements of operator $\hat{A}$. The formal inverse of the Fourier transform in Eq. (1) gives the angle dependence of the classical function as a Fourier series,

$$A_{\rm cl}(\bar{n},q) = \sum_{k\in\mathbb{Z}^F} e^{ikq}\left\langle n+\frac{k}{2}\middle|\hat{A}\middle|n-\frac{k}{2}\right\rangle. \qquad (2)$$

Here, however, the procedure becomes nonunique (and nonexact) because the classical action variable $\bar{n}$ has to interpolate for all real numbers, while the matrix elements are only defined for integer values of $n\pm\frac{k}{2}$.

One way to proceed is to use the spin-matrix mapping (SMM) method of Meyer and Miller (MM),[47,48] which utilizes the fact that a general two-state system is equivalent to a spin $\frac{1}{2}$ system. Thus any 2×2 matrix $A_{n,n'}$, $n,n'\in\{0,1\}$, can be written as a linear combination of the three spin matrices $\mathbf{S}_x$, $\mathbf{S}_y$, and $\mathbf{S}_z$ (and the 2×2 identity matrix). One then uses the classical expressions for the spin angular momentum,

$$S_x = \sqrt{\sigma^2-m^2}\cos(q) \qquad (3a)$$

$$S_y = \sqrt{\sigma^2-m^2}\sin(q) \qquad (3b)$$

$$S_z = m. \qquad (3c)$$

in terms of the action-angle variables (m,q). The quantum values of the action variable m (the projection quantum number) are $\pm\frac{1}{2}$, but it is convenient to have the quantum values of the action variables be 0 (unoccupied) and 1 (occupied). The elementary canonical transformation $n=m+\frac{1}{2}$ makes this change, giving the classical function of action-angles (n,q) for a general 2×2 matrix A as

$$A(n,q) = (1-n)\,A_{00} + n\,A_{11} + \sqrt{n-n^2+\lambda}\left(A_{10}\,e^{iq} + A_{01}\,e^{-iq}\right) \qquad (4)$$

where $\lambda=\sigma^2-\frac{1}{4}$. The value of σ^2 will be discussed below.

To employ this approach on a given second-quantized Hamiltonian, MW used this SMM model for each term in a Hamiltonian. The Hamiltonian in the present work has terms of the form $\hat{a}_i^\dagger\hat{a}_i$ and $\hat{a}_i^\dagger\hat{a}_j$. The matrix elements of the operator $\hat{a}_i^\dagger\hat{a}_i$ are diagonal,

$$\left\langle n'\middle|\hat{a}_i^\dagger\hat{a}_i\middle|n\right\rangle = n_i\prod_j \delta_{n'_j,n_j}, \qquad (5a)$$

which corresponds to Eq. (4) with $A_{00}=0$ and $A_{11}=1$ for the ith degree of freedom, and to the identity matrix for all other degrees of freedom. The SMM model thus gives

$$\hat{a}_i^\dagger\hat{a}_i \mapsto = n_i. \qquad (5b)$$

The matrix elements for $\hat{a}_i^\dagger\hat{a}_j$ are

$$\left\langle n'\middle|\hat{a}_i^\dagger\hat{a}_j\middle|n\right\rangle = \delta_{n'_i,n_i+1}\delta_{n'_j,n_j-1} \times\prod_{k\neq i,j}\delta_{n'_k,n_k}\prod_{p=i+1}^{j-1}(-1)^{n_p} \qquad (6a)$$

where we have assumed that $i<j$. In the case $i>j$, the product over p goes from $j+1$ to $i-1$: it always includes the states between (but not including) i and j. That product is the result of the anticommutation relation of fermionic creation/annihilation operators.

These matrix elements are separable products of 2×2 matrices: for the ith degree of freedom (corresponding to

the factor $\delta_{n_i',n_i'+1}$) the 2×2 matrix has $A_{10}=1$ as the only nonzero matrix element, so that Eq. (4) gives the corresponding classical function as

$$\sqrt{n_i - n_i^2 + \lambda}\, e^{iq_i}. \tag{6b}$$

For the jth degree of freedom (i.e., the factor δ_{n_j',n_j-1}), the only nonzero matrix element is $A_{01}=1$, resulting in the classical function

$$\sqrt{n_j - n_j^2 + \lambda}\, e^{-iq_j}. \tag{6c}$$

For each degree of freedom p, with p between i and j (in normal ordered form), the factor $\delta_{n_p',n_p}(-1)^{n_p}$ from Eq. (6a) corresponds to a diagonal 2×2 matrix in Eq. (4) with $A_{00}=1$ and $A_{11}=-1$. This SMM method thus gives the classical function

$$1-2n_p. \tag{6d}$$

The net result is

$$\hat{a}_i^\dagger \hat{a}_j \mapsto \sqrt{(n_i - n_i^2 + \lambda)\left(n_j - n_j^2 + \lambda\right)}\, e^{i(q_i - q_j)} \times \prod_{p=i}^{j} f_b(n_p) \tag{7}$$

where the SMM method gives $f_b(n_p) = 1-2n_p$. For the present application, however, we found that using these factors $f_b(n_p)$ significantly underestimates the current (see section V), while excellent results were obtained by omitting these factors, i.e., by setting $f_b(n_p)=1$. We also tried an alternative, $f_b(n_p)=\exp(i\pi n_p)$, but it had the same defect. The issue seems to be that with the quantum values of $n_p \in \{0,1\}$, the product of these factors is ± 1, while the classical value of n_p frequently leads to $f_b(n_p)<1$. The product of many such factors leads to factors much less than 1, and thus off-diagonal coupling that are much too small.

We now return to the value of σ (which determines λ). For a classical spin with $s=\frac{1}{2}$, $\sigma^2 = s^2 = \frac{1}{4}$, such that $\lambda = 0$. However, MM suggested using the Langer modified value $\sigma^2 = \left(s+\frac{1}{2}\right)^2 = 1$, giving $\lambda = \frac{3}{4}$. Here, we suggest instead using the quantum value of $\sigma^2 = s(s+1) = \frac{3}{4}$, and thus $\lambda = \frac{1}{2}$. The results in section V give empirical reasons for this choice.

The choice $\lambda = \frac{1}{2}$ also can be justified with the following argument. Because the goal is to generate a mapping that accounts for the correct dynamics, it is reasonable to try to match the short-time dynamics of a simple problem. Consider the Hamiltonian $\hat{H} = k\left(\hat{a}_A^\dagger \hat{a}_B + \hat{a}_B^\dagger \hat{a}_A\right)$, with initial population in state A. The first time derivative of the initial ($t=0$) quantum population of state A is zero, as is that of our semiclassical model (averaged over angles). The second derivative of the initial quantum population of state A is $-2k^2$, while the semiclassical model gives $-4k^2\lambda$. If these are to be equal, then we must set $\lambda = \frac{1}{2}$.

To summarize, the modifications we have made to the original MW model are (1) to use a value of $\lambda = \frac{1}{2}$ rather than the previously suggested Langer modified value of $\frac{3}{4}$, and (2) to set the factors $f_b(n_p)$ in equation (7) to unity.

B. Intial conditions

The semiclassical mapping also requires the selection of initial conditions for the action-angle variables. It is clear that a naïve approach based on the classical mapping described above will not provide the correct statistical treatment: Even for the one-particle system $\hat{H} = \hat{a}^\dagger \hat{a} \mapsto n$, it does not reproduce the quantum partition function when the action-angle variables are sampled from the corresponding classical thermal distribution.

To recover the correct statistical behavior (at least at time $t=0$) we use a quasi-classical procedure. Since we are interested in a noncorrelated initial state with thermally populated leads and an unpopulated quantum dot, we can populate each degree of freedom independently. We enforce quantum statistics on the initial conditions for each degree of freedom i by setting the initial action n_i to either 0 or 1 such that the expectation value of the action $\langle n_i \rangle$, averaged over the set of initial conditions, satisfies the Fermi distribution,

$$f(\epsilon_i - \mu_i) = \left(1 + e^{\beta(\epsilon_i - \mu_i)}\right)^{-1} \tag{8}$$

where μ_i is the chemical potential of the lead in which mode i is located and $\beta = 1/T$ is the inverse temperature. The angle variable q_i is selected at random between 0 and 2π.

III. MODEL HAMILTONIAN

We use the resonant level (Landauer) model as an example of quantum transport. It consists of a single quantum dot state coupled to two electrodes (left and right) according to the Hamiltonian

$$\hat{H} = \epsilon_0 \hat{a}_0^\dagger \hat{a}_0 + \sum_{k=1}^{N} \epsilon_k \hat{a}_k^\dagger \hat{a}_k + \sum_{k=1}^{N} t_k \left(\hat{a}_0^\dagger \hat{a}_k + \hat{a}_k^\dagger \hat{a}_0\right), \tag{9}$$

where ϵ_0 is the energy of the isolated quantum dot (and will also be used to model a gate voltage), ϵ_k is the energy associated with the electrode mode k, and t_k is the coupling between the quantum dot and the electrode mode k.

Using the procedure described in section II, we construct the classical model of this Hamiltonian in action-

angle variables:

$$H(n,q) = \epsilon_0 n_0 + \sum_{k=1}^{N} \epsilon_k n_k + \sum_{k=1}^{N} t_k \sqrt{n_0 - n_0^2 + \frac{1}{2}} \times \sqrt{n_k - n_k^2 + \frac{1}{2}} \left(e^{i(q_0 - q_k)} \prod_{p=1}^{N} f_b(n_p) + \text{H.c} \right). \tag{10}$$

The left current is given by the change in occupancy of the left electrode, with the right current defined analogously and the total current given by half the difference of the two. For the Hamiltonian in Eq. (9), the Heisenberg time derivative gives the left current as:

$$\hat{I}_L(t) = -e \frac{\mathrm{d}}{\mathrm{d}t} \left\langle \sum_{k \in L} \hat{a}_k^\dagger \hat{a}_k \right\rangle \tag{11}$$

$$= -\frac{e\,i}{\hbar} \left\langle \sum_{k \in L} t_k \left(\hat{a}_0^\dagger \hat{a}_k - \hat{a}_k^\dagger \hat{a}_0 \right) \right\rangle \tag{12}$$

where L is the set of states in the left electrode.

We can choose to take the semiclassical approximation before the time derivative by mapping the occupation to a classical quantity and taking its time derivative, or we can take the result of the quantum time derivative and map that to a classical quantity. For this system, our mapping method gives formally equivalent results for either procedure.

The electrodes are described within the wide band limit with a sharp cutoff at high and low energy values:

$$J_{L/R}(\epsilon) = \frac{\Gamma_{L/R}}{\left(1 + e^{A\left(\epsilon - \frac{B}{2}\right)}\right)\left(1 + e^{-A\left(\epsilon + \frac{B}{2}\right)}\right)} \tag{13}$$

where, in all results reported below we use $\Gamma_L = \Gamma_R = \frac{1}{2}$, $\Gamma = \Gamma_L + \Gamma_R$, $A = 5\Gamma$, and $B = 20\Gamma$. For the semiclassical mapping, we use a uniform discretization to select the energies of the leads' states, and thus the couplings are given by

$$t_k(\epsilon_k) = \sqrt{\frac{J(\epsilon_k)\Delta\epsilon}{2\pi}}. \tag{14}$$

IV. EXACT QUANTUM MECHANICS

An exact quantum mechanical solution for the transient current for the Hamiltonian specified above is straightforward to derive, and thus provides means to assess the accuracy of the semiclassical treatment. Under the assumptions of no correlation at $t = 0$

$$\left\langle a_k^\dagger(0)\, a_0(0) \right\rangle = \left\langle a_0^\dagger(0)\, a_k(0) \right\rangle = 0, \tag{15}$$

and a Boltzmann distribution for the leads' populations

$$\left\langle a_k^\dagger(0)\, a_{k'}(0) \right\rangle = f(\epsilon_k - \mu_{L,R})\, \delta_{kk'}, \tag{16}$$

where $f(\epsilon)$ is the Fermi function and as before $\mu_{L,R}$ is the chemical potential for the left (L) or right (R) lead, one can derive an exact expression for the left current given in Eq. (12):

$$I_L(t) = \frac{2e}{\hbar} \mathrm{Im} \left\{ \frac{1}{2\pi} \int_{-\infty}^{\infty} e^{-i\omega' t} J_L(\omega')\, \mathrm{d}\omega' \right\} \tag{17}$$

for any given initial dot population

$$\left\langle a_0^\dagger(0)\, a_0(0) \right\rangle = n_0 \in [0,1]. \tag{18}$$

In the above, $J_L(\omega')$ is given by:

$$J_L(\omega') = \frac{1}{2\pi} \int_{-\infty}^{\infty} \left(\frac{1}{-i\omega'} \frac{\left(-\frac{i}{2}\Sigma_L^<(\omega) + \left(-\frac{i}{2}\Sigma_L^<(\omega - \omega')\right)^\dagger\right)}{\left(\omega - \frac{\epsilon_0}{\hbar} - \frac{1}{\hbar}\Sigma_{L,R}(\omega)\right)} - \frac{\left(\Sigma_L(\omega - \omega')\right)^\dagger n_0(0)}{\left(\omega - \omega' - \frac{\epsilon_0}{\hbar} - \frac{1}{\hbar}\left(\Sigma_{L,R}(\omega - \omega')\right)^\dagger\right)\left(\omega - \frac{\epsilon_0}{\hbar} - \frac{1}{\hbar}\Sigma_{L,R}(\omega)\right)} + \frac{1}{-i\omega'\hbar} \frac{\left(\Sigma_L(\omega - \omega')\right)^\dagger \left(-\frac{i}{2}\Sigma_{L,R}^<(\omega) + \left(-\frac{i}{2}\Sigma_{L,R}^<(\omega - \omega')\right)^\dagger\right)}{\left(\omega - \omega' - \frac{\epsilon_0}{\hbar} - \frac{1}{\hbar}\left(\Sigma_{L,R}(\omega - \omega')\right)^\dagger\right)\left(\omega - \frac{\epsilon_0}{\hbar} - \frac{1}{\hbar}\Sigma_{L,R}(\omega)\right)} \right) \mathrm{d}\omega, \tag{19}$$

$\Sigma(\omega)$ is the self energy, and $\Sigma^<(\omega)$ is the lesser self energy, both specified below. A similar expression can be derived for the right current ($I_R(t)$) by the replacement $L \leftrightarrow R$. The total current is given by the different of the left and right currents, $I(t) = \frac{I_L(t) - I_R(t)}{2}$.

As a check on the above, we discuss two known limits for the current. In the limit $t \to 0$, it is simple to show that the current vanishes. This is a result of the initial

preparation of an uncorrelated state and can be derived with the help of the initial value theorem

$$\lim_{t\to 0} I_L(t) = \frac{2e}{\hbar}\mathrm{Im}\left\{\lim_{-i\omega'\to\infty} -i\omega' J(\omega')\right\} = 0, \qquad (20)$$

where we assumed that the self-energies vanish at the boundaries in the frequency domain:

$$\lim_{-i\omega'\to\infty} \Sigma(\omega) = \lim_{-i\omega'\to\infty} \Sigma^{<}(\omega) = 0. \qquad (21)$$

To recover the Landauer expression for the current at steady state[3,4] we take the limit $t\to\infty$ in Eq. (17), this time with the aid of the final value theorem

$$\begin{aligned}\lim_{t\to\infty} I_L(t) &= \frac{2e}{\hbar}\mathrm{Im}\left\{\lim_{-i\omega'\to 0} -i\omega' J(\omega')\right\} \\ &= \frac{2e}{\hbar}\mathrm{Im}\left\{\frac{1}{2\pi}\int_{-\infty}^{\infty}\left(\frac{\left(\frac{i}{2}\Sigma_L^{<}(\omega)+\left(\frac{i}{2}\Sigma_L^{<}(\omega)\right)^{\dagger}\right)}{\left(\omega-\frac{\epsilon_0}{\hbar}-\frac{1}{\hbar}\Sigma_{L,R}(\omega)\right)}\right.\right. \\ &\quad \left.\left. + \frac{1}{\hbar}\frac{\left(\Sigma_L(\omega)\right)^{\dagger}\left(\frac{i}{2}\Sigma_{L,R}^{<}(\omega)+\left(\frac{i}{2}\Sigma_{L,R}^{<}(\omega)\right)^{\dagger}\right)}{\left(\omega-\frac{\epsilon_0}{\hbar}-\frac{1}{\hbar}\left(\Sigma_{L,R}(\omega)\right)^{\dagger}\right)\left(\omega-\frac{\epsilon_0}{\hbar}-\frac{1}{\hbar}\Sigma_{L,R}(\omega)\right)}\right)\mathrm{d}\omega\right\}. \qquad (22)\end{aligned}$$

Rearranging Eq. (22) and using the well known representation of the self energies in terms of the real ($\Lambda_{L,R}(\omega)$) and imaginary ($\Gamma_{L,R}(\omega)$) portions:

$$\Sigma_{L,R}(\omega) = \Lambda_{L,R}(\omega) - \frac{1}{2}i\Gamma_{L,R}(\omega) \qquad (23)$$

$$\Sigma_{L,R}^{<}(\omega) = if(\hbar\omega-\mu_{L,R})\Gamma_{L,R}(\omega) \qquad (24)$$

we finally arrive at the Landauer expression for the current:

$$\begin{aligned}\lim_{t\to\infty} I_L(t) &= \frac{e}{2\pi\hbar^2}\int_{-\infty}^{\infty}\left(f(\hbar\omega-\mu_L)-f(\hbar\omega-\mu_R)\right) \\ &\quad\times\frac{\Gamma_R(\omega)\Gamma_L(\omega)}{\left(\omega-\frac{\tilde{\epsilon_0}}{\hbar}\right)^2+\frac{1}{4\hbar^2}\Gamma(\omega)^2}\mathrm{d}\omega \qquad (25)\end{aligned}$$

where the rescaled energy $\tilde{\epsilon_0}$ is given by:

$$\tilde{\epsilon_0} = \epsilon_0 + \Lambda_L(\omega) + \Lambda_R(\omega) \qquad (26)$$

and $\Gamma(\omega) = \Gamma_L(\omega) + \Gamma_R(\omega)$.

We choose

$$\Gamma_{L/R}(\omega) = \frac{\Gamma_{L/R}}{\left(e^{A\left(\omega-\frac{B}{2}\right)}+1\right)\left(e^{-A\left(\omega+\frac{B}{2}\right)}+1\right)} \qquad (27)$$

where $\Gamma_L = \Gamma_R = \frac{1}{2}$. A and B are defined in Eq. (13). $\Lambda_{L/R}(\omega)$ is obtained from the Kramers-Kronig relation

$$\Lambda_{L/R}(\omega) = \frac{1}{\pi}\mathrm{pp}\int_{-\infty}^{\infty}\mathrm{d}\omega'\,\frac{\Gamma_{L/R}(\omega')}{\omega'-\omega} \qquad (28)$$

where pp denotes the Cauchy principle value.

V. RESULTS

Our simulations used the semiclassical Hamiltonian of Eq. (10) in action-angle variables, with initial conditions selected as described in section II. Numerical integration of the trajectories was performed with the sixth-order Gear predictor-corrector algorithm, modified to allow adaptive timesteps (necessary due to the square roots in the Hamiltonian). The maximum step size was $\Delta t = 0.01\hbar/\Gamma$. We used 400 states per lead and reported results with 2×10^5 trajectories (see below for further discussion on these points). A calculation to time $t = 8\hbar/\Gamma$ with 400 modes per electrode and 2×10^5 trajectories required less than one hour walltime with 120 computational cores.

In Figs. 1-3, we plot the left (lower panels), right (middle panels) and total (upper panels) currents as a function of time for different source-drain voltages (Fig. 1), gate voltages (Fig. 2) and temperatures (Fig. 3). The left, right and total currents show a distinct time-dependence and decay to the same value at steady state. In these plots, the exact quantum results of section IV are presented as lines, and the results of the semiclassical model presented in section II are presented as symbols.

Figure 1 shows the time-dependent current at a wide range of source-drain voltages $eV = \mu_L - \mu_R$, with $\epsilon_0 = 0$ (zero gate voltage) and temperature $T = \Gamma/3$. The largest values of this bias are limited by the width of our band, $B = 20\Gamma$ [see Eq. (13)]. The most striking result shown in Fig. 1 is the excellent agreement between the semiclassical method and the exact quantum mechanical result. In some cases it is difficult to distinguish the two.

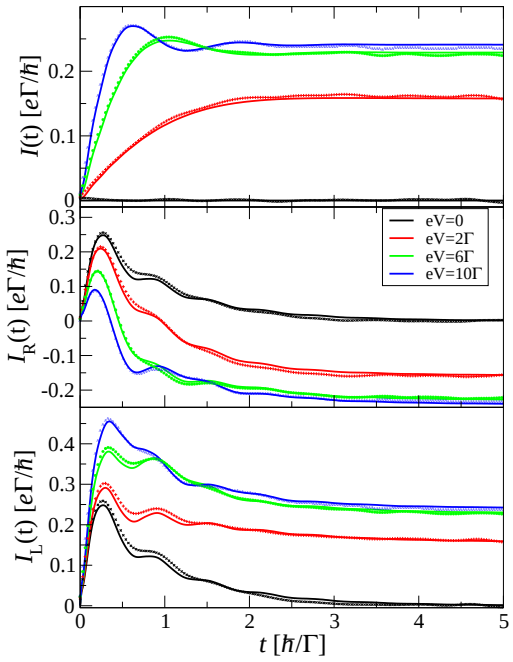

Figure 1. Plots of the left (lower panel), right (middle panel) and total (upper panel) transient current for different values of the source-drain voltage $eV = \mu_L - \mu_R$. Other model parameters are: $T = \Gamma/3$, $\epsilon_0 = 0$ and $N_L = N_R = 400$. Solid line and symbols correspond to exact quantum mechanical and semiclassical results, respectively.

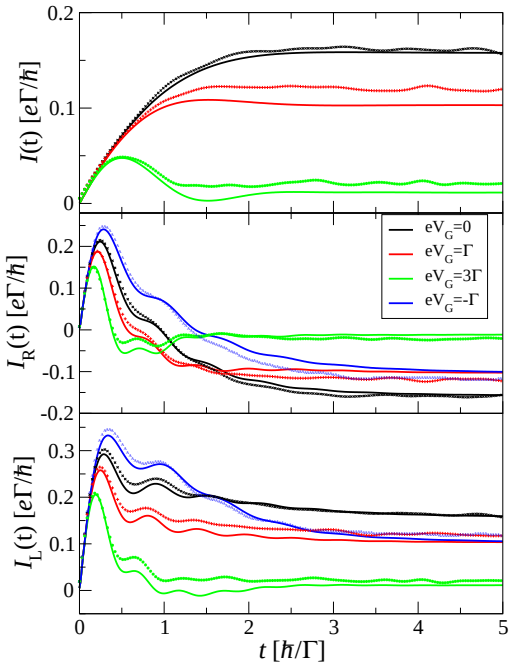

Figure 2. Plots of the left (lower panel), right (middle panel) and total (upper panel) transient current for different values of the gate voltage $eV_g = \epsilon_0$. Other model parameters are: $\mu_L = -\mu_R = \Gamma$, $T = \Gamma/3$ and $N_L = N_R = 400$. Solid line and symbols correspond to exact quantum mechanical and semiclassical results, respectively.

The semiclassical approach captures both the evolution of the current at early and intermediate times, and its decay to the correct steady-state value at longer time. The agreement is quantitative for all source-drain voltages studied. The pronounced oscillations in the left and right current as they decay to steady state result from the finite band width of the leads, and are also captured by the semiclassical method.

At zero source-drain bias, the left and right currents show a significant transient effect until the zero-current steady-state value is reached, while the total current is identically zero at all times. This suggests that for other systems the total current would be a better observable since one can infer the steady-state result from relatively shorter times.[49,50] For the largest bias presented, $I = 0.241\Gamma$, which approaches the infinite bias limit of $I = 0.25\Gamma$.

In Fig. 2 we plot the time-dependent current for different gate voltages, eV_G. The gate voltage is determined by the parameter $eV_G = \epsilon_0$ in the Hamiltonian (9). The line for $eV_G = -\Gamma$ is not plotted for the total current because the quantum result overlaps the $eV_G = \Gamma$ line (the semiclassical results for these two series nearly overlap as well). For nonzero gate voltages, we find that the semiclassical method is not as accurate as for the case where $eV_G = 0$, although it still captures the correct trends at all times. In particular, the even more pronounced oscillations and the decay of the amplitude of the oscillations are captured by the semiclassical treatment. Additionally, the steady-state currents for gate voltages of equal magnitude but opposite signs (e.g., $eV_G = \pm\Gamma$) are equal (within the numerical noise), just as in the quantum mechanical results for these parameters.

The effect of temperature is shown in Fig. 3. We explored a range temperatures from $\Gamma/5$ to 2Γ, which covers the classical to quantum regimes. We find excellent agreement for all temperatures, even when considering the left and right currents which exhibit transient phenomena on longer timescales and are thus more difficult to describe.[49] A closer examination of the results reveals that the semiclassical treatment is a bit more accurate for higher temperatures (as might be expected), yet the overall agreement for all temperatures is quite surprising, in particular in view of the failures of semiclassical treatments at low temperatures for other systems.[42]

Fig. 4 deals with the choices we made in the semiclassical procedure described in section II. The upper left panel displays the effect of choosing different values of

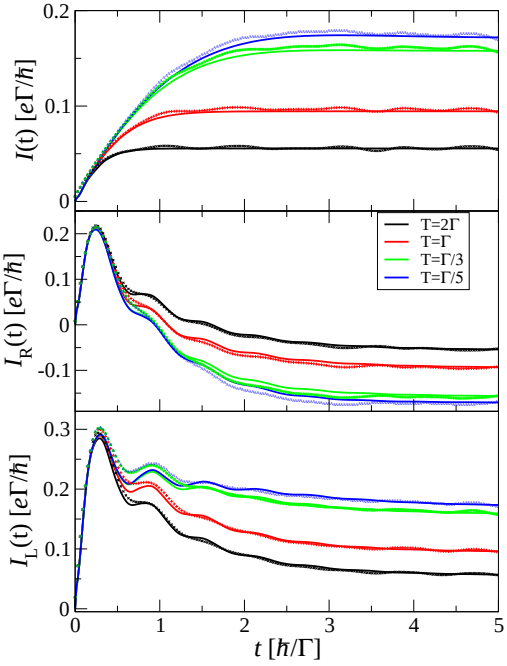

Figure 3. Plots of the left (lower panel), right (middle panel) and total (upper panel) transient current for different temperatures. Other model parameters are: $\mu_L = -\mu_R = \Gamma$, $\epsilon_0 = 0$ and $N_L = N_R = 400$. Solid line and symbols correspond to exact quantum mechanical and semiclassical results, respectively.

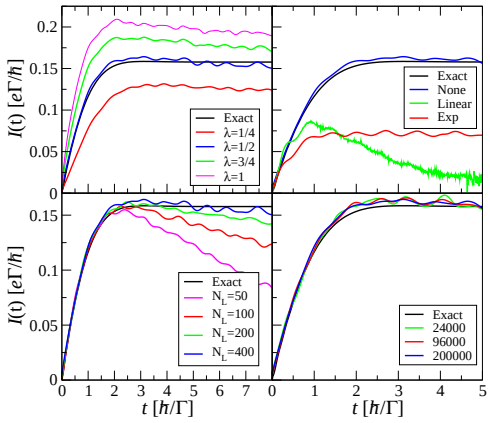

Figure 4. Plots of the total transient current for different values of the Langer modification (upper left panel), for different choices of the factor $f_b(n)$ (upper right panel), for different numbers of states in the leads (lower left panel), and with different numbers of trajectories (lower right panel). In all panels $\mu_L = -\mu_R = \Gamma$, $\epsilon_0 = 0$, $T = \Gamma/3$ and $N_L = N_R$.

λ (or, equivalently, σ^2). The choice $\lambda = \frac{1}{2}$ corresponds to the quantum $\sigma^2 = s(s+1)$, and is what was used in the results shown in Figs. 1–3. The choice $\lambda = \frac{3}{4}$ is the the Langer-modified $\sigma^2 = (s+\frac{1}{2})^2$ suggested by MW. Stock has treated the Langer modification as a free parameter,[51] and so in that spirit we include the choices $\lambda = 1$ and $\lambda = \frac{1}{4}$, the latter being near Stock's result of 0.3125 (for a different system). In particular, note the short-time behavior: The slope of the semiclassical current at time $t = 0$ can be shown to be proportional to λ, and $\lambda = \frac{1}{2}$ best matches the exact quantum result. This is consistent with the short-time analysis in section II.

The upper right panel of Fig. 4 shows how the function $f_b(n)$, which relates to the anticommutation relations, affects the results. The SMM form for these factors, $f_b(n) = 1 - 2n$, is labeled as "Linear," while the alternate we explored, $f_b(n) = \exp(i\pi n)$, is labeled "Exp." The method we used in the results presented in Figs. 1–3 was to omit these terms (i.e., $f_b(n) = 1$) and is labelled "None." Clearly, the linear and exponential versions underestimate the current (the linear version tending to zero steady-state current), while omitting these factors gives extremely good agreement. This can be traced to the fact that quantum mechanically, the values of these factors are either -1 or 1 which can be absorbed into the coupling constants t_k as a phase factor. One can prove that the current is independent of the sign of t_k for the initially uncorrelated case. However, in the semiclassical mapping the values of these factors are continuous. They can therefore significantly change the effective value of the coupling constants, decreasing the current. It is also notable that the oscillations in the linear and exponential versions are more pronounced than when these factors are omitted.

The lower left panel shows the importance of using a sufficient number of modes per electrode. Since the semiclassical simulations are performed for a finite number of states in the electrodes, the "steady-state" current we obtain cannot hold to infinite time. All other results presented involved 400 modes per electrode, which Fig. 4 suggests holds the steady state until at least time $t \approx 5\hbar/\Gamma$.

The lower right panel of Fig. 4 shows how the results converge with the number of trajectories. Even at 2.4×10^4 trajectories, the approximate result is clear. The results presented in Figs. 1–3 are with 2×10^5 trajectories.

VI. CONCLUDING REMARKS

The present classical model for electronic degrees of freedom (dofs) is seen to provide an excellent description of the dynamics of electron transmission in a simple model of a molecular transistor driven out of equilibrium. The near quantitative results, obtained over a wide range of system parameters (including quite low temperatures), are especially remarkable since the model is implemented with our rather crude quasi-classical approach:

Quantized initial conditions are selected for the action-angle variables, but then the dynamics are completely classical (i.e., generated by Hamilton's equations, without any more sophisticated *semi*classical input). One is accustomed to quasi-classical treatments being semi-quantitative, e.g., for quantized vibrational and rotational dofs — and even for electronically nonadiabatic transitions between two or three electronic states — but the level of accuracy seen in the present work is much better than that reported in such cases. It may be that the dense set of electronic states that constitute the left and right electrodes in the present molecular model leads to a rapid decay of the initial factorized state to the steady state, and thus makes the overall system behave more classically.

The present results encourage one to expand the treatment to more realistic molecular models of such phenomena. It is obvious how to include nuclear degrees of freedom in the classical molecular dynamics simulations along with the classical model for the electronics dofs. Also, MW's classical electronic model is able to include electron correlation, i.e., two electron interactions in the second-quantized Hamiltonian of the type

$$\sum_{i,j,k,l} \langle ij|\,|kl\rangle\, \hat{a}_i^\dagger \hat{a}_j^\dagger \hat{a}_l \hat{a}_k, \tag{29}$$

which would be necessary to describe effects such as Coulomb blockade. Though the form of this more general classical electronic model has been given, it has never been applied to any nontrivial examples. It will be of interest to see how well the approach will work for such more realistic molecular models.

VII. ACKNOWLEDGMENTS

This work was supported by the US-Israel Binational Science Foundation, by the FP7 Marie Curie IOF project HJSC, by the National Science Foundation Grant No. CHE-0809073 and by the Director, Office of Science, Office of Basic Energy Sciences, Chemical Sciences, Geosciences, and Biosciences Division, U.S. Department of Energy under Contract No. DE-AC02-05CH11231. We also acknowledge a generous allocation of supercomputing time from the National Energy Research Scientific Computing Center (NERSC) and the use of the Lawrencium computational cluster resource provided by the IT Division at the Lawrence Berkeley National Laboratory. TL is grateful to the The Center for Nanoscience and Nanotechnology at Tel Aviv University of a doctoral fellowship. GC is grateful to the Azrieli Foundation for the award of an Azrieli Fellowship. ER thanks the Miller Institute for Basic Research in Science at UC Berkeley for partial financial support via a Visiting Miller Professorship.

REFERENCES

[1] A. Nitzan and M. A. Ratner, Science **300**, 1384 (2003).
[2] A. J. Leggett, S. Chakravarty, A. T. Dorsey, M. Fisher, A. Garg, and W. Zwerger, Rev. Mod. Phys. **59**, 1 (1987).
[3] R. Landauer, Philos. Mag. **21**, 863 (1970).
[4] M. Büttiker, Phys. Rev. Lett. **57**, 1761 (1986).
[5] D. C. Langreth and E. Abrahams, Phys. Rev. B **24**, 2978 (1981).
[6] H. Haug and A. P. Jauho, *Quantum Kinetics in Transport and Optics of Semiconductors* (Springer, Germany, 1996).
[7] S. Datta, *Electronic Transport in Mesoscopic Systems* (Cambridge University Press, Cambridge, 1995).
[8] S. R. White, Phys. Rev. Lett. **69**, 2863 (1992).
[9] P. Schmitteckert, Phys. Rev. B **70**, 121302 (2004).
[10] F. B. Anders and A. Schiller, Phys. Rev. Lett. **95**, 196801 (2005).
[11] L. Mühlbacher and E. Rabani, Phys. Rev. Lett. **100**, 176403 (2008).
[12] S. Weiss, J. Eckel, M. Thorwart, and R. Egger, Phys. Rev. B **77**, 195316 (2008).
[13] P. Werner, T. Oka, and A. J. Millis, Phys. Rev. B **79**, 035320 (2009).
[14] M. Schiró and M. Fabrizio, Phys. Rev. B **79**, 153302 (2009).
[15] D. Segal, A. J. Millis, and D. R. Reichman, Phys. Rev. B **82**, 205323 (2010).
[16] G. Cohen and E. Rabani, "Nonequilibrium many-body projected dynamics at long time scales with real-time path integral monte carlo," In preparation.
[17] D. V. Averin and K. K. Likharev, J. Low Temp. Phys. **62**, 345 (1986).
[18] C. W. J. Beenakker, Phys. Rev. B **44**, 1646 (1991).
[19] J. Koch and F. von Oppen, Phys. Rev. Lett. **94**, 206804 (2005).
[20] Y. Meir and N. S. Wingreen, Phys. Rev. Lett. **68**, 2512 (1992).
[21] P. Werner, T. Oka, M. Eckstein, and A. J. Millis, Phys. Rev. B **81**, 035108 (2010).
[22] M. Galperin, M. A. Ratner, and A. Nitzan, J. Phys.: Condens. Matter **19**, 103201 (2007).
[23] J. C. Tully, J. Chem. Phys. **93**, 1061 (1990).
[24] F. J. Webster, P. J. Rossky, and R. A. Friesner, Comput. Phys. Commun. **63**, 494 (1991).
[25] D. F. Coker and L. Xiao, J. Chem. Phys. **102**, 496 (1995).
[26] R. Kapral, Ann. Rev. Phys. Chem. **57**, 129 (2006).
[27] W. H. Miller, J. Phys. Chem. A **105**, 2942 (2001).
[28] W. H. Miller, J. Chem. Phys. **125**, 132305 (2006).
[29] N. Makri, J. Phys. Chem. A **108**, 806 (2004).
[30] H. Wang, X. Sun, and W. H. Miller, J. Chem. Phys. **108**, 9726 (1998).
[31] N. Makri and K. Thompson, Chem. Phys. Lett. **291**, 101 (1998).
[32] H. Wang, X. Y. Song, D. Chandler, and W. H. Miller, J. Chem. Phys. **110**, 4828 (1999).
[33] K. Thompson and N. Makri, J. Chem. Phys. **110**, 1343 (1999).
[34] E. Rabani, S. A. Egorov, and B. J. Berne, J. Phys. Chem. A **103**, 9539 (1999).
[35] H. Wang, M. Thoss, and W. H. Miller, J. Chem. Phys. **112**, 47 (2000).
[36] M. Thoss, H. Wang, and W. H. Miller, J. Chem. Phys. **114**, 9220 (2001).
[37] A. Nakayama and N. Makri, J. Chem. Phys. **119**, 8592 (2003).
[38] A. Nakayama and N. Makri, Proc. Natl. Acad. Sci. USA **102**, 4230 (2005).
[39] E. Martin-Fierro and E. Pollak, J. Chem. Phys. **126**, 164108 (2007).
[40] J. Liu and W. H. Miller, J. Chem. Phys. **128**, 144511 (2008).
[41] J. M. Moix and E. Pollak, J. Chem. Phys. **129**, 064515 (2008).
[42] S. A. Egorov, E. Rabani, and B. J. Berne, J. Phys. Chem. B **103**, 10978 (1999).
[43] M. Thoss and H. B. Wang, Ann. Rev. Phys. Chem. **55**, 299 (2004).
[44] W. H. Miller and K. A. White, J. Chem. Phys. **84**, 5059 (1986).
[45] W. H. Miller and C. W. McCurdy, J. Chem. Phys **69**, 5163 (1978).

[46]C. W. McCurdy, H. D. Meyer, and W. H. Miller, J. Chem. Phys. **70**, 3177 (1979).
[47]H. Meyer and W. H. Miller,.
[48]H. Meyer and W. H. Miller, J. Chem. Phys **72**, 2272 (1980).
[49]O. Hod, R. Baer, and E. Rabani, J. Phys.: Cond. Mat. **20**, 383201 (2008).
[50]M. Caspary, L. Berman, and U. Peskin, Chem. Phys. Lett **369**, 232 (2003).
[51]G. Stock, J. Chem. Phys. **103**, 2888 (1995).